

Raman spectroscopy of graphene and graphite: Disorder, electron–phonon coupling, doping and nonadiabatic effects

Andrea C. Ferrari*

Cambridge University, Engineering Department, 9 JJ Thomson Avenue, Cambridge CB3 0FA, UK

Accepted 22 March 2007 by A. Geim

Available online 27 April 2007

Abstract

We review recent work on Raman spectroscopy of graphite and graphene. We focus on the origin of the *D* and *G* peaks and the second order of the *D* peak. The *G* and *2D* Raman peaks change in shape, position and relative intensity with number of graphene layers. This reflects the evolution of the electronic structure and electron–phonon interactions. We then consider the effects of doping on the Raman spectra of graphene. The Fermi energy is tuned by applying a gate-voltage. We show that this induces a stiffening of the Raman *G* peak for both holes and electrons doping. Thus Raman spectroscopy can be efficiently used to monitor number of layers, quality of layers, doping level and confinement.

© 2007 Elsevier Ltd. All rights reserved.

PACS: 63.20.Dj; 63.20.Kr; 71.15.Mb; 78.30.-j

Keywords: A. Graphene; A. Carbon; C. Structure; E. Raman spectroscopy

1. Introduction

Graphene is the two-dimensional (2D) building block for carbon allotropes of every other dimensionality. It can be stacked into 3D graphite, rolled into 1D nanotubes, or wrapped into 0D fullerenes. Its recent discovery [1–3] completes the carbon-family. This finally opens the opportunity to study experimentally its electronic and phonon properties, which so far had to be inferred from theory.

In general, carbon-based materials play a major role in today's science and technology and the discovery of graphene is the last of a long string of continuous advances in the science of carbon. These include, for example, the chemical vapour deposition of diamond [4], the discovery of fullerenes [5] and carbon nanotubes [6–8], and mastering the properties of amorphous and disordered carbons [9–12], to span, on demand, almost all the range from graphite to diamond to carbon polymers [9–17]. Indeed, amorphous and diamond-like carbons (DLC) are currently used in many every-day life applications, such as, for example,

magnetic hard disk coatings, wear protective and anti-reflective coatings for tribological tools, engine parts, razor blades and sunglasses, biomedical coatings (such as hips or stents) and microelectro-mechanical systems [9,10]. Graphitic carbon and, to an extent, carbon nanotubes, are also utilized in batteries [18]. Applications in field emission displays, microwave amplifiers, transistors, supercapacitors, structural and conductive composites, photonic devices although all well beyond the proof-of-principle stage, have yet to make it to market. One of the main advantages of graphene is the possible advent of a planar technology, compatible with existing manufacturing processes [1].

A key requirement for carbon research and applications is the ability to identify and characterize all the members of the carbon family, both at the lab- and at mass-production scale. To be appealing, a characterization tool must be nondestructive, fast, with high resolution and give the maximum structural and electronic information. Raman spectroscopy provides all these. It is the backbone of research in such diverse fields, ranging from physics, to engineering, chemistry and biology. Indeed, most of the papers published every year on carbon materials have at least a Raman spectrum in them [19].

Raman spectroscopy can thus become the standard also in the fast growing field of graphene. One should remember that

* Tel.: +44 1223 748351; fax: +44 1223 748348.

E-mail address: acf26@hermes.cam.ac.uk.

in the process of making graphene, be it from mechanical cleavage [1,2], “exfoliated growth” [20,21], chemical vapour deposition [21,22], chemical exfoliation [23], all sorts of carbon species can in principle occur, similarly to what happens when making nanotubes. Unwanted by-products and structural damage can also be created while shaping graphene into devices. It would thus be advisable to have a structural reference, monitored, for example, by Raman spectroscopy, as common denominator to compare the materials used by different groups. This is standard practice in the field of nanotubes and amorphous and diamond-like carbons [19]. In the case of nanotubes, other optical structural characterization techniques, such as photoluminescence excitation spectroscopy, are now very popular [24], as ellipsometry or XPS are in amorphous and diamond like carbons [25]. It is thus foreseeable that other optical techniques (maybe even simpler than Raman spectroscopy) will become available also for graphene, once the field expands experimentally.

The toll for the simplicity of Raman measurements is paid when it comes to spectral interpretation. The Raman spectra of all carbon systems show only a few prominent features, no matter the final structure, be it a conjugated polymer or a fullerene [19]. The spectra appear deceptively simple: just a couple of very intense bands in the 1000–2000 cm^{-1} region and few other second-order modulations. However, their shape, intensity and positions allow to distinguish a hard amorphous carbon, from a metallic nanotube, giving as much information as that obtained by a combination of other lengthy and destructive approaches [19]. The peculiar dispersion of the π electrons in graphene is the fundamental reason why Raman spectroscopy in carbons is always resonant and, thus, a powerful and efficient probe of their electronic properties, not only of their vibrations [19]. This explains why the interpretation of the Raman spectra of graphitic materials was investigated for almost 40 years [19,26] and why intense effort has been put towards the Raman measurement of few-layer graphite samples [27,28], even before the discovery of graphene.

2. D and G peaks, double resonance and Kohn anomalies

Fig. 1 compares the Raman spectra of a few representative carbon materials: graphite, metallic and semiconducting nanotubes and high and low sp^3 amorphous carbons, all measured for visible excitation. Fig. 2 plots the D peak position as a function of excitation energy for defected graphite.

The main features in the Raman spectra of carbons are the so-called G and D peaks, which lie at around 1560 and 1360 cm^{-1} respectively for visible excitation. In amorphous carbons a peak at around 1060 cm^{-1} (T peak) is seen in UV excitation [14]. Except for UV excitation, the Raman spectra of carbon films are dominated by the sp^2 sites, because visible excitation always resonates with the π states. Thus even for highly sp^3 amorphous carbon samples the visible Raman spectra are due to sp^2 vibrations. Only for diamond or samples containing a significant fraction of diamond phase, the diamond sp^3 peak at 1332 cm^{-1} is seen [31]. The cross-section for

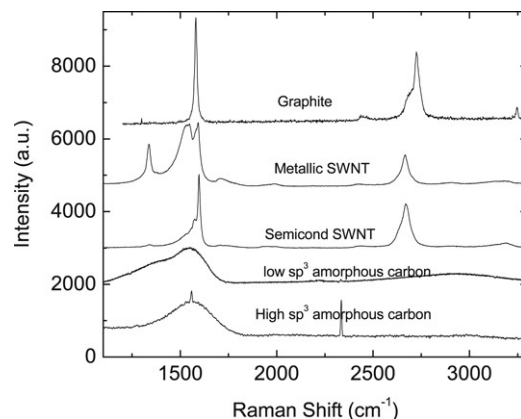


Fig. 1. Raman spectra of graphite, metallic and semiconducting carbon nanotubes, low and high sp^3 amorphous carbons.

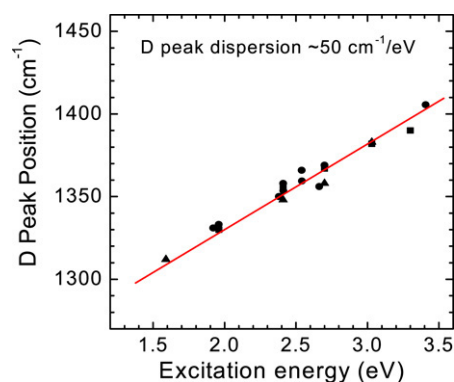


Fig. 2. D peak dispersion as function of excitation energy [39].

the amorphous sp^3 C–C vibrations is negligible for visible excitation, thus its Raman signature can only be seen for UV excitation [14]. Indeed, the cross-section for graphite at 514 nm is ~ 55 times higher than that of diamond [32] and hydrogenated amorphous carbon has a 230 times higher cross-section than diamond [33].

The assignment of the D and G peaks is straightforward in the “molecular” picture of carbon materials. These bands are present in all poly-aromatic hydrocarbons [34,35]. The G peak is due to the bond stretching of all pairs of sp^2 atoms in both rings and chains. The D peak is due to the breathing modes of sp^2 atoms in rings [13,26,34]. However, the “solid-state” approach to the interpretation of these bands has undergone a debate, which lasted several decades, with some aspects yet to be clarified.

The D peak was first attributed to an A_{1g} breathing mode at K, activated by the relaxation of the Raman fundamental selection rule $\mathbf{q} = \mathbf{0}$ [26]. It was then linked to maxima in the vibrational density of states of graphite at M and K points [36, 37]. However, this does not account for the dispersion of the D position with photon energy (Fig. 2 [38,39]), why the D peak overtone at $\sim 2710 \text{ cm}^{-1}$, seen even where no D peak is present, is dispersive, or why the $I(D)/I(G)$ ratio is dispersive [38,39]. Phonon confinement does not explain why the D mode is more intense than other modes closer to Γ with smaller $\Delta\mathbf{q}$. It also does not explain why the D mode is seen in disordered graphite

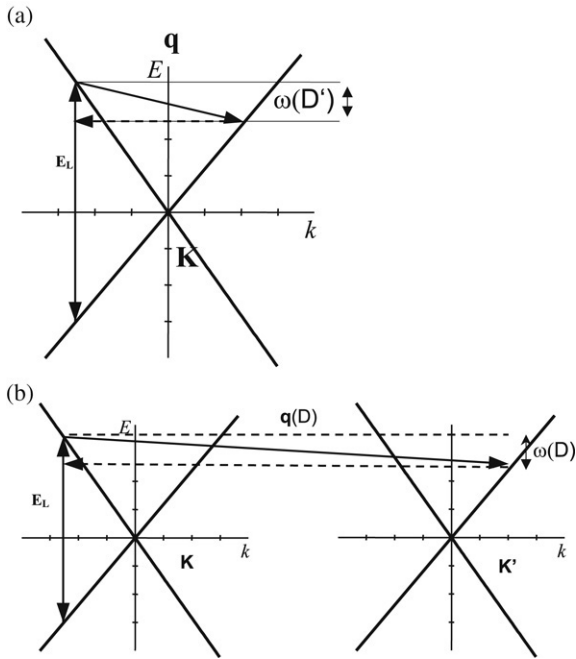


Fig. 3. Double resonance scheme for the D' peak (close to Γ) and the D peak (close to \mathbf{K}) [41]. E_L is the incident laser energy.

with in plane correlation length, L_a , as big as 30 nm [40], while Heisenberg indetermination would limit the participating phonons to a much narrower $\Delta\mathbf{q}$ range around Γ [13].

Ref. [39] empirically proposed that the D peak arises as resonant Raman coupling, in which there is a strong enhancement of the Raman cross-section of a phonon of wavevector \mathbf{q} , when it equals the wavevector \mathbf{k} of the electronic transition excited by the incident photon ($\mathbf{k} = \mathbf{q}$ “quasi-selection rule” [13]). However, the physical reason for this “quasi-selection rule” was unclear and this did not yet explain why, amongst all phonons satisfying this condition, only those on one particular optical branch are seen.

Refs. [41,42] identified double resonance (DR), as the activation mechanism.

Within DR, Raman scattering is a fourth order process [41], Fig. 3. The activation process for the D peak is shown in Fig. 3(b). (i) a laser induced excitation of an electron/hole pair; (ii) electron–phonon scattering with an exchanged momentum $q \sim K$; (iii) defect scattering; (iv) electron/hole recombination. The DR condition is reached when the energy is conserved in all these transitions [41]. A similar process to Fig. 3(b) is possible intra-valley, as shown in Fig. 3(a). This activates phonons with a small \mathbf{q} , resulting in the so-called D' peak, which can be seen around $\sim 1620 \text{ cm}^{-1}$ in defected graphite [36].

Besides the activation mechanism, the phonon dispersion around K is crucial for the correct interpretation of the Raman D peak. Once established that this peak is attributed to phonon branches around K [26,37,43–47,13,14,19,41], its dispersion with excitation energy will depend on the precise shape of these branches [41,48].

Graphene has four possible phonon branches around K (the three shown in Fig. 4, plus a lower lying optical branch crossing the K point at $\sim 800 \text{ cm}^{-1}$), and they should all be

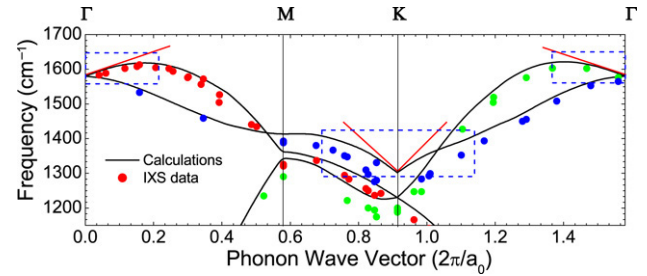


Fig. 4. Calculated phonon dispersion of graphene, from Ref. [48], compared with the experimental data on graphite from Ref. [47].

Raman active if their Electron Phonon Couplings (EPC) are ignored [41,39,44–46]. But, it is a fact that only the D peak has significant intensity [26]. In the molecular approach [43,13,14], the D peak is assigned to the branch starting from the $\mathbf{K}-A'_1$ mode, based on its symmetry and on its large Raman cross-section in aromatic molecules of increasing size. However, this attribution was initially disputed. In fact, the measured linear D peak dispersion (Fig. 2) seemed at odds with the flat, or even negative, slope of the highest optical branch near K , given by previous calculations [43,49–52]. Because of this, initially many authors [39,44,41,45,46] assigned the D peak to the doubly degenerate linearly dispersive $1200 \text{ cm}^{-1} E'$ mode at \mathbf{K} . Ref. [48] finally confirmed the attribution of the D peak to the highest optical branch starting from the $\mathbf{K}-A'_1$ mode [26,43,13,14]. Indeed, the A'_1 branch has, by far, the biggest electron–phonon coupling amongst the K phonons [53]. Second, this branch is linearly dispersive, Fig. 4. A Kohn anomaly at \mathbf{K} is the physical origin of this dispersion, which is in agreement with the measured D peak dispersion of Fig. 2 [39].

In general, atomic vibrations are partially screened by electronic states. In a metal this screening can change rapidly for vibrations associated to certain points of the Brillouin Zone (BZ), entirely determined by the shape of the Fermi surface. The consequent anomalous behaviour of the phonon dispersion is called Kohn anomaly [54]. Kohn anomalies may occur only for wavevectors \mathbf{q} such that there are two electronic states \mathbf{k}_1 and $\mathbf{k}_2 = \mathbf{k}_1 + \mathbf{q}$ both on the Fermi surface [54]. In graphene, the gap between occupied and empty electronic states is zero at the two BZ points \mathbf{K} and \mathbf{K}' . Since $\mathbf{K}' = 2\mathbf{K}$, these are connected by the vector \mathbf{K} . Thus, Kohn anomalies can occur for $\mathbf{q} = \Gamma$ or $\mathbf{q} = \mathbf{K}$. Ref. [48] demonstrated that graphene has two significant Kohn anomalies for $\Gamma-E_{2g}$ and $\mathbf{K}-A'_1$, Fig. 4.

It is thus impossible to derive the phonon branches at Γ and \mathbf{K} by force constant approaches based on a finite number of force constants, as often done [43,45,46,49–51].

These results have also implications for carbon nanotubes. Due to their reduced dimensionality, metallic tubes display much stronger Kohn anomalies than graphite. This gives phonon softening, implying that folded graphite does not reproduce the phonon dispersions of metallic tubes [55,53,51]. The presence of Kohn anomalies in metallic tubes makes their Raman spectra different from semiconducting tubes [53,55].

To summarize, the current understanding is that the D peak is due to LO phonons around K [13,26], is active by double

resonance [41,42] and is strongly dispersive with excitation energy due to the Kohn Anomaly at K [48].

3. Electron–phonon coupling from phonon dispersions and Raman line widths

Electron–phonon coupling (EPC) is a key physical parameter in graphene and nanotubes. Ballistic transport, superconductivity, excited state dynamics, Raman spectra and phonon dispersions all fundamentally depend on it. In nanotubes, the optical phonons EPC are also extremely relevant since electron scattering by optical phonons sets the ultimate limit to high field ballistic transport [56–60]. Many tight-binding calculations of optical phonons EPC in graphene and nanotubes are reported in literature, with contrasting results [57, 58,61–65] (see Table II of Ref. [55] for a summary).

Refs. [48,53] presented DFT calculations of the graphene optical phonons EPC, and, most importantly, a strategy for the experimental determination of the EPCs. Ref. [48] proved that a simple analytical description of the Kohn anomalies in graphene is possible. The anomalies are revealed by two sharp kinks in the phonon dispersion, Fig. 4. The slope of these kinks is proportional to the ratio of the square of the electron–phonon coupling matrix element and the π bands slope at \mathbf{K} [48]:

$$\text{Slope}^{\text{LO}}(\Gamma) = \frac{\sqrt{3}a_0^2}{8M\omega_\Gamma} \cdot \frac{\text{EPC}(\Gamma)^2}{v_F} \quad (1)$$

$$\text{Slope}(K) = \frac{\sqrt{3}a_0^2}{8M\omega_K} \cdot \frac{\text{EPC}(K)^2}{v_F} \quad (2)$$

where M is the carbon atomic mass, $a_0 = 2.46 \text{ \AA}$ is the graphite lattice spacing, $v_F = 8.38 \times 10^5 \text{ m/s}$ is the Fermi velocity from DFT and $\hbar\omega_\Gamma = 196 \text{ meV}$ [48]. Note that recent experimental determinations of v_F give $9.1 \times 10^5 \text{ m/s}$ [66] $-1.1 \times 10^6 \text{ m/s}$ [67], in excellent agreement with DFT. Furthermore [48]:

$$\frac{\text{Slope}^{\text{LO}}(\Gamma)\omega_\Gamma}{\text{Slope}(K)\omega_K} = 2. \quad (3)$$

The phonons around Γ were measured by several groups with close agreement [68–70,47]. Fig. 4 compares the calculated phonon dispersion of Ref. [48] with the most recent Inelastic X ray scattering data from Ref. [47]. From Eq. (1) and a quadratic fit to the data of Ref. [47], we get $\text{Slope}^{\text{LO}}(\Gamma) \sim 133 \text{ cm}^{-1} \text{ \AA}$, and, thus, the experimental $\text{EPC}(\Gamma) \sim 39 \text{ (eV/\AA)}^2$. The agreement with the DFT value $\sim 46 \text{ (eV/\AA)}^2$ is excellent. The experimental phonon dispersions around K are more scattered, so Eq. (3) can be used to estimate $\text{EPC}(K)$ from $\text{EPC}(\Gamma)$.

An alternative strategy for EPC measurement is based on the analysis of the G peak linewidths. The optical phonons EPC are the major source of broadening for the Raman G band in graphite, graphene and for the G^- peak in metallic nanotubes [53,55]. In a perfect crystal, the line-width of a phonon γ is determined by its interaction with other elementary excitations. Usually, $\gamma = \gamma^{\text{an}} + \gamma_0^{\text{EPC}}$, where γ^{an} is due to the interaction with other phonons and γ_0^{EPC} with electron–hole

pairs. γ^{an} is given by anharmonic terms in the interatomic potential and is always there. γ^{EPC} is determined by the EPC and is present only in systems where the electron gap is zero. If the anharmonic contribution is negligible or otherwise known, measuring the line width is the simplest way to determine the EPC. From the Fermi golden rule the EPC contribution to the G peak FWHM is given by a simple analytical formula [53]:

$$\gamma_0^{\text{EPC}} = \frac{\sqrt{3}a_0^2}{4M} \cdot \frac{\text{EPC}(\Gamma)^2}{v_F^2}. \quad (4)$$

Provided the conservation of energy and momentum is fulfilled (i.e. $q \leq \omega_\Gamma/v_F$). Otherwise, $\gamma_0^{\text{EPC}} = 0$. This is satisfied by the G peak of undoped graphite and graphene. On the other hand, the double resonant D' mode close to Γ does not satisfy this. Indeed, the D' peak is sharper than the G peak [71].

The experimental $\text{FWHM}(G)$ was measured on a single-crystal graphite $\sim 13 \text{ cm}^{-1}$ [55,72]. Temperature-dependent measurements show no increase of $\text{FWHM}(G)$ in the 2–900 K range [72]. Accounting for the Raman spectrometer resolution of $\sim 1.5 \text{ cm}^{-1}$, this implies an an-harmonic contribution lower than the spectral resolution. Thus, $\gamma^{\text{EPC}}(G) \sim 11.5 \text{ cm}^{-1}$. Then, from Eq. (5), $\text{EPC}(\Gamma)^2 \sim 47 \text{ (eV/\AA)}^2$. This compares very well with DFT, again confirming that $\gamma^{\text{an}}(G)$ is small. If we combine (4) with (1) we get:

$$v_F = \frac{2\text{Slope}^{\text{LO}}(\Gamma)\omega_\Gamma}{\gamma^{\text{EPC}}}. \quad (5)$$

This provides a direct measurement of the Fermi velocity in terms of experimental quantities related to the phonon spectrum. For the experimental data reported here we get $v_F \sim 7 \times 10^5 \text{ m/s}$ in excellent agreement with direct experimental determinations from ARPES or magneto-transport [66,67].

Finally Refs. [30,73] extended Eq. (4) for finite doping ($\varepsilon_F \neq 0$, being ε_F the Fermi level):

$$\gamma^{\text{EPC}}(\varepsilon_F) = \gamma_0^{\text{EPC}} \{ f[-(\hbar\omega_\Gamma/2 + \varepsilon_F)] - f(\hbar\omega_\Gamma/2 - \varepsilon_F) \} \quad (6)$$

where $f(x)$ is the Fermi–Dirac distribution of argument x .

Note that, even for zero doping, Eq. (6) predicts a significant γ^{EPC} decrease with temperature. Since the anharmonic contribution to the FWHM is much smaller than γ^{EPC} , Eq. (7) predicts a net decrease of $\text{FWHM}(G)$ with temperature, which we recently observed [72]. This is different from what happens in most materials, where FWHM always increase with temperature.

4. The Raman spectrum of graphene and graphene layers

Fig. 5 compares the Raman spectra of graphene and bulk graphite measured at 514.5 nm excitation [29]. The two most intense features are the G peak at 1580 cm^{-1} and a band at $\sim 2700 \text{ cm}^{-1}$, historically named G' , since it is the second most prominent band always observed in graphite samples [38]. However we now know that this band is the second order of the D peak. Thus we believe it is more convenient to refer to it as $2D$ peak [29]. Fig. 5 also shows another peak at $\sim 3250 \text{ cm}^{-1}$. Its frequency is higher than double the G peak frequency, thus

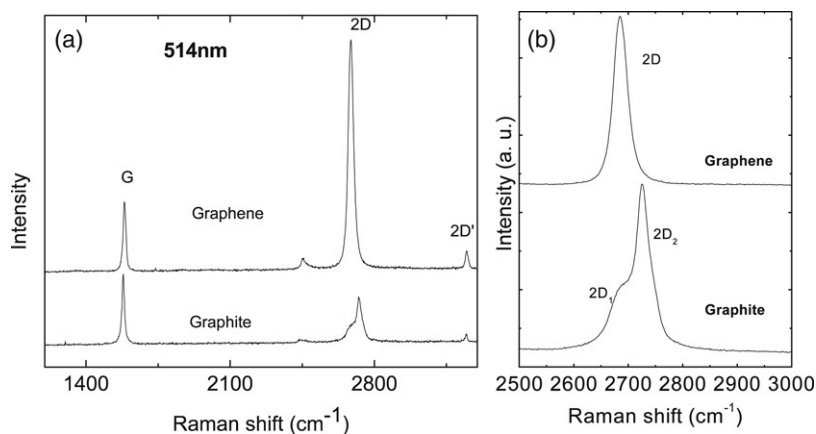


Fig. 5. (a) Comparison of the Raman spectra of graphene and graphite measured at 514.5 nm. (b) Comparison of the $2D$ peaks in graphene and graphite.

it is not its second order. This peak, is in fact the second order of the intra-valley D' peak of Fig. 3(a), thus, for consistency, we call it $2D'$.

Fig. 5(b) shows a significant change in the shape and intensity of the $2D$ peak of graphene compared to bulk graphite. The $2D$ peak in bulk graphite consists of two components $2D_1$ and $2D_2$ [36,38], roughly $1/4$ and $1/2$ the height of the G peak, respectively. Graphene has a single, sharp $2D$ peak, roughly four times more intense than the G peak [29]. The original results of Ref. [29] were then confirmed in the similar experiments reported in refs. [74,75]. However, the layer counting in [74,75] was not independently confirmed by TEM, unlike Ref. [29]. The uncertain number of layers is quite evident in Ref. [74], where similar Raman spectra are reported for a varying number of layers.

Fig. 6 plots the evolution of the $2D$ band as a function of the number of layers for 514.5 nm and 633 nm excitations. These immediately indicate that bi-layer graphene has a much broader and upshifted $2D$ band with respect to graphene. This band is also quite different from bulk graphite. It has four components, $2D_{1B}$, $2D_{1A}$, $2D_{2A}$, $2D_{2B}$, two of which, $2D_{1A}$ and $2D_{2A}$, have higher relative intensities than the other two, as indicated in Fig. 7. Fig. 6(c) and (d) show that a further increase of the number of layers leads to a significant decrease of the relative intensity of the lower frequency $2D_1$ peaks. For more than five layers the Raman spectrum becomes hardly distinguishable from that of bulk graphite. Thus Raman spectroscopy can clearly identify a single layer, from bi-layer from few (less than five) layers. This also explains why previous experiments on nano-graphites, but not individual or bi-layer graphene, did not identify these features [28,76].

SWNTs show a sharp $2D$ peak similar to that of graphene [77], Fig. 1. Despite the similarities, it is important to note that there are major differences between the graphene and SWNT Raman spectra, which allow to easily distinguish these materials. Indeed, confinement and curvature split the two degenerate modes of the G peak in SWNTs, resulting in G^+ and G^- peaks, [55,77], in contrast to graphene.

Ref. [29] explained why graphene has a single $2D$ peak, and why this splits in four components in bi-layer graphene, which then evolve in only two components in bulk graphite. Several

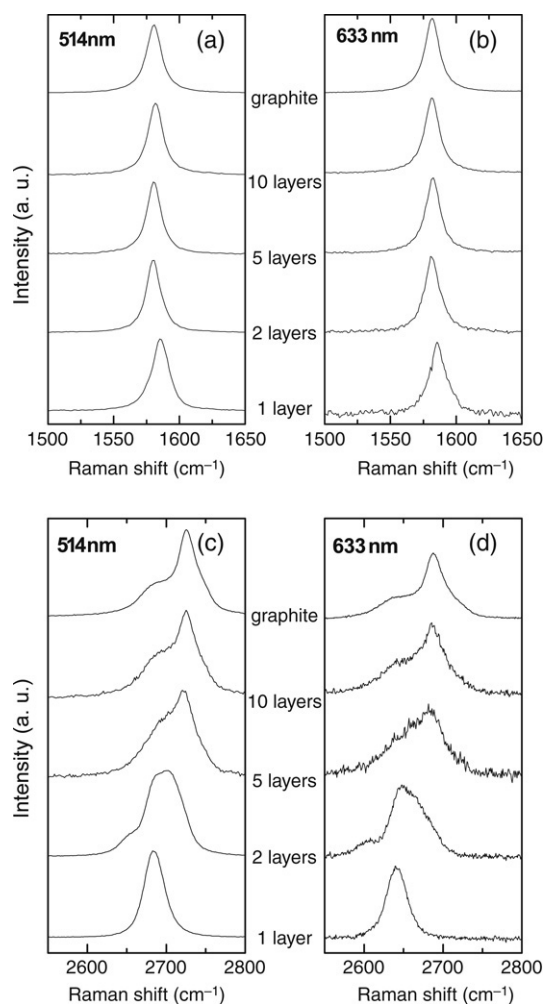


Fig. 6. (a) and (b) Evolution of G peak as a function of number of layers for 514 and 633 nm excitations, (c) and (d) Evolution of the $2D$ peak as a function of number of layers for 514 and 633 nm excitations.

authors previously attempted to explain the double structure of the $2D$ peak in graphite [38,36,39,28,78], however they always neglected the evolution of the electronic bands with the number of layers, which is, on the contrary, a key fact.

The $2D$ peak in graphene is due to two phonons with opposite momentum in the highest optical branch near the \mathbf{K}

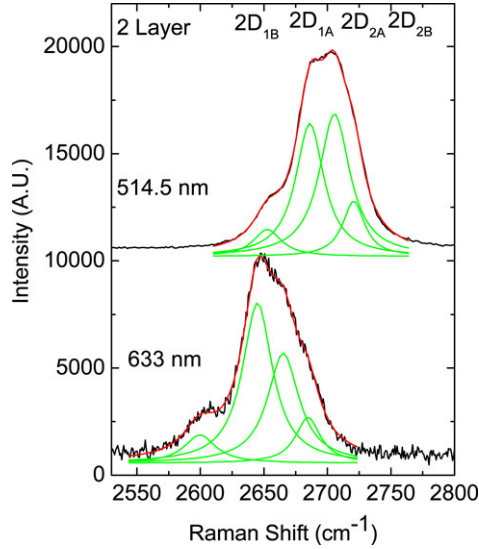


Fig. 7. The four components of the 2D peak in bi-layer graphene.

point of the Brillouin zone (A'_1 symmetry at \mathbf{K}). Fig. 6(c) and (d) show that this peak changes in position with varying excitation energy, at twice the rate of the first order D peak. This is due to double resonance, which links the phonon wavevectors to the electronic band structure [41]. The resulting 2D Raman frequency is twice the frequency of the scattering phonon, whose q is determined by the DR condition. Fig. 3(b) can be used for the 2D peak, but substituting the electron-defect scattering with electron-phonon scattering with an exchanged momentum $-\mathbf{q}$, which allows to satisfy the Raman fundamental selection rule for second order scattering ($\mathbf{q} + (-\mathbf{q}) = 0$). Only phonons satisfying DR conditions with momentum $q > K$, along the Γ - \mathbf{K} - \mathbf{M} direction ($K < q < M$) contribute [29]. The other two possible DR phonons, with $q < K$ and $q \sim K$, give a much smaller contribution to the Raman intensity. In fact, the $q < K$ phonon involves a smaller portion of the phase-space because of the band-structure trigonal warping and the $q \sim K$ phonon has a zero electron-phonon coupling for this transition, as discussed in Ref. [48].

The four components of the 2D peak for the bi-layer could, in principle, be attributed to two different mechanisms: the splitting of the phonon branches [13,36,38,40] or the splitting of the electronic bands [13]. From DFT [48,29] the splitting of the phonon branches is $< 1.5 \text{ cm}^{-1}$, much smaller than the experimentally observed 2D splitting. Thus, this is solely due to electronic bands effects. In the bi-layer, the interaction of the graphene planes causes the π and π^* bands to divide in four bands, with a different splitting for electrons and holes. The incident laser light can couple only two pairs of the four bands [29]. On the contrary, the two almost degenerate phonons in the highest optical branch can couple all the electron bands amongst them. The resulting four processes involve phonons with momenta q_{1B} , q_{1A} , q_{2A} , and q_{2B} , corresponding to phonons with different frequencies, due to the strong dispersion of the phonon bands around \mathbf{K} . These produce the four peaks in the Raman spectrum of bi-layer graphene. However, the phonons q_{1A} and q_{2A} scatter between bands of the same type and are associated to processes more intense than q_{1B} and q_{2B} ,

since the portion of the phase space where the DR condition is satisfied is larger [29].

5. The Raman spectrum of doped graphene: Breakdown of the adiabatic Born–Oppenheimer approximation

Doping changes the Fermi surface of graphene. This moves the Kohn anomaly away from $\mathbf{q} = 0$. Thus, since first order non-double resonant Raman scattering probes $\mathbf{q} = 0$ phonons, intuitively we expect a stiffening of the G peak. Indeed, refs. [30,79] reported that the G peak of graphene responds to doping. The doping level was controlled by applying a gate voltage. The G peak upshifts for both holes and electron doping [30,79].

Fig. 8(a) and (b) reports the G peak position and FWHM measured at 200 K. The trend of FWHM is fully consistent with the prediction of Eq. (6). The upshift of the G peak with doping can be fully understood only by extending the DFT calculations of Ref. [48] to include beyond Born–Oppenheimer corrections to the dynamic matrix [30]. The detailed theoretical analysis of this case is reported in Refs. [73,80,81].

The adiabatic Born–Oppenheimer approximation (ABO) is standard to describe the interaction between electrons and nuclei since the early days of quantum mechanics [82–84]. ABO assumes that the lighter electrons adjust adiabatically to the motion of the heavier nuclei, remaining at any time in their instantaneous groundstate. ABO is well justified when the energy gap between ground and excited electronic states is larger than the energy scale of the nuclear motion. The use of ABO to describe lattice motion in metals is, therefore, questionable. In spite of this, ABO has proven effective for the accurate determination of chemical reactions, molecular dynamics and phonon frequencies in a wide range of metallic systems.

Quite remarkably ABO fails in graphene [30]. Indeed, the inverse of the G -peak pulsation is ~ 3 fs, which is much smaller than the typical electron-momentum relaxation time. This is due to impurity, electron–electron and electron–phonon scattering with non-zero momentum phonons and was estimated as few hundreds fs from electron-mobility in graphene [85] and ultra-fast spectroscopy in graphite [86,87]. Thus electrons do not have time to relax their momenta to reach the instantaneous adiabatic ground state, as assumed in ABO. At zero T , the G peak shifts can be described analytically [73]:

$$\hbar \Delta\omega(G) = \frac{AEPC(\Gamma)^2}{\pi M \omega_0(G) \hbar v_F^2} \times \left[|\varepsilon_F| + \frac{\hbar \omega_0(G)}{4} \ln \left(\frac{|\varepsilon_F| - \frac{\hbar \omega_0(G)}{2}}{|\varepsilon_F| + \frac{\hbar \omega_0(G)}{2}} \right) \right] \quad (7)$$

where $A = 5.24 \text{ \AA}^2$ is the graphene unit cell area and $\omega_0(G)$ is the frequency of the G peak in the undoped case. The result of Eq. (7) can be extended to finite temperature, see Ref. [30,73]. Fig. 8 show the excellent agreement of the nonadiabatic finite T calculations with experiments.

Due to double resonance, the D peak will still be described by ABO, even in the presence of moderate doping, since the D

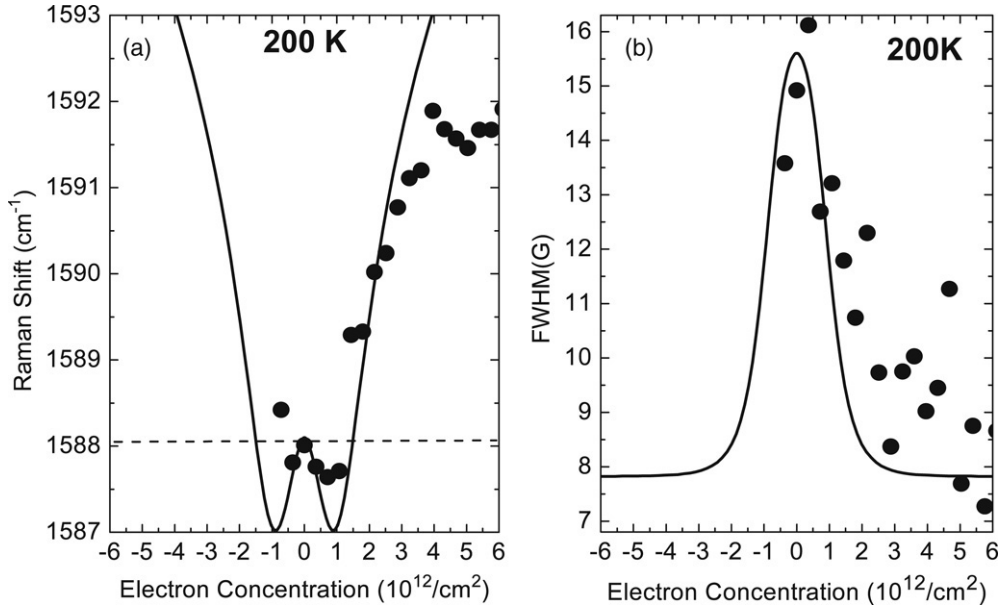


Fig. 8. (a) G peak position as a function of electron concentration at 200 K. (dots) measurements; (horizontal-dashed line) adiabatic Born–Oppenheimer; (line) finite-temperature nonadiabatic calculation. The minimum observed in the calculations at $\sim 10^{12} \text{ cm}^{-2}$ occurs when the Fermi Energy equals half of the phonon energy. (b) $\text{FWHM}(G)$ at 200 K as a function of electron concentration. (dots) measured; (line) theoretical FWHM of a Voigt profile obtained from a Lorentzian component given by Eq. (7), and a constant Gaussian component of $\sim 8 \text{ cm}^{-1}$ [30].

peak phonons are away from K , unlike the G peak phonon, which is always at $\mathbf{q} = \mathbf{0}$. For significant doping levels, however, the effects of charge transfer will be felt. High hole doping results in phonon stiffening, while high electron doping causes phonon softening [73,88]. The total response to doping will be the sum of the charge transfer and nonadiabatic effects. In practice, for doping levels below 0.6 eV, this just results in a slight asymmetry of the G peak stiffening [73]. Thus, since the G peak always stiffens, while the $2D$ peak responds differently to holes and electron doping [89], by monitoring both G and $2D$ it is in principle possible to estimate the doping level.

Another consequence of doping is the significant decrease of $I(2D)/I(G)$, with respect to the doped case [89].

Fig. 9 show that, for the same nonintentionally doped graphene sample, we can have different G peak positions and FWHM , as well as different $I(2D)/I(G)$. This indicates that inhomogeneous self-doping can happen. Indeed, if the inhomogeneity happens over scales smaller than the Raman spot size, an asymmetrical G peak can be seen [90].

This also happens when comparing the Raman spectra of a graphene sample on a substrate, to that of a suspended sample [29,90]. Even though the general features are the same, the G peak is slightly downshifted and broader for the suspended case, while the $2D$ peak is much more intense. This is consisted with the decrease of self-doping upon removal of the substrate [90]. However, the suspended sample also shows a D peak. This indicates a small increase of disorder, as explained in the next section.

6. Disordered graphite and graphene

In order to compare different samples and devices, or different locations on the same sample, another crucial

parameter, besides doping, is the amount of disorder. For multilayers assessing turbostraticity is also important.

We introduced a three-stage classification of disorder, leading from graphite to amorphous carbons [13,14], which allows to simply assess all the Raman spectra of carbons. The Raman spectrum is considered to depend on:

- (i) clustering of the sp^2 phase;
- (ii) bond disorder;
- (iii) presence of sp^2 rings or chains;
- (iv) the sp^2/sp^3 ratio.

These factors act as competing forces on Raman spectra. We defined an *amorphization trajectory* [13,14] ranging from graphite to highly sp^3 amorphous carbon in three stages:

- (1) Graphite \rightarrow nanocrystalline graphite;
- (2) nanocrystalline graphite \rightarrow low sp^3 amorphous carbon;
- (3) low sp^3 amorphous carbon \rightarrow high sp^3 amorphous carbon.

In the study of graphene, stages 1 and 2 are the most relevant and are thus summarized here

(A) Stage 1: Graphite \rightarrow nanocrystalline graphite

The seminal paper studying disorder in graphitic samples is that of Tuinstra and Koenig (TK) [26]. They noted that the ratio of the D peak intensity to that of the G peak varied inversely with L_a :

$$\frac{I(D)}{I(G)} = \frac{C(\lambda)}{L_a} \quad (8)$$

where $C(488 \text{ nm}) \sim 4.4 \text{ nm}$ from Refs. [26,91,92,44]. There are few experimental verifications of TK where L_a is known independently by X-ray diffraction (XRD) [26,93–97], and the minimum L_a for which TK has been directly verified is $\sim 2 \text{ nm}$. TK assumes that graphite becomes uniformly nanocrystalline. However, for a system with mixed grain sizes, with volume

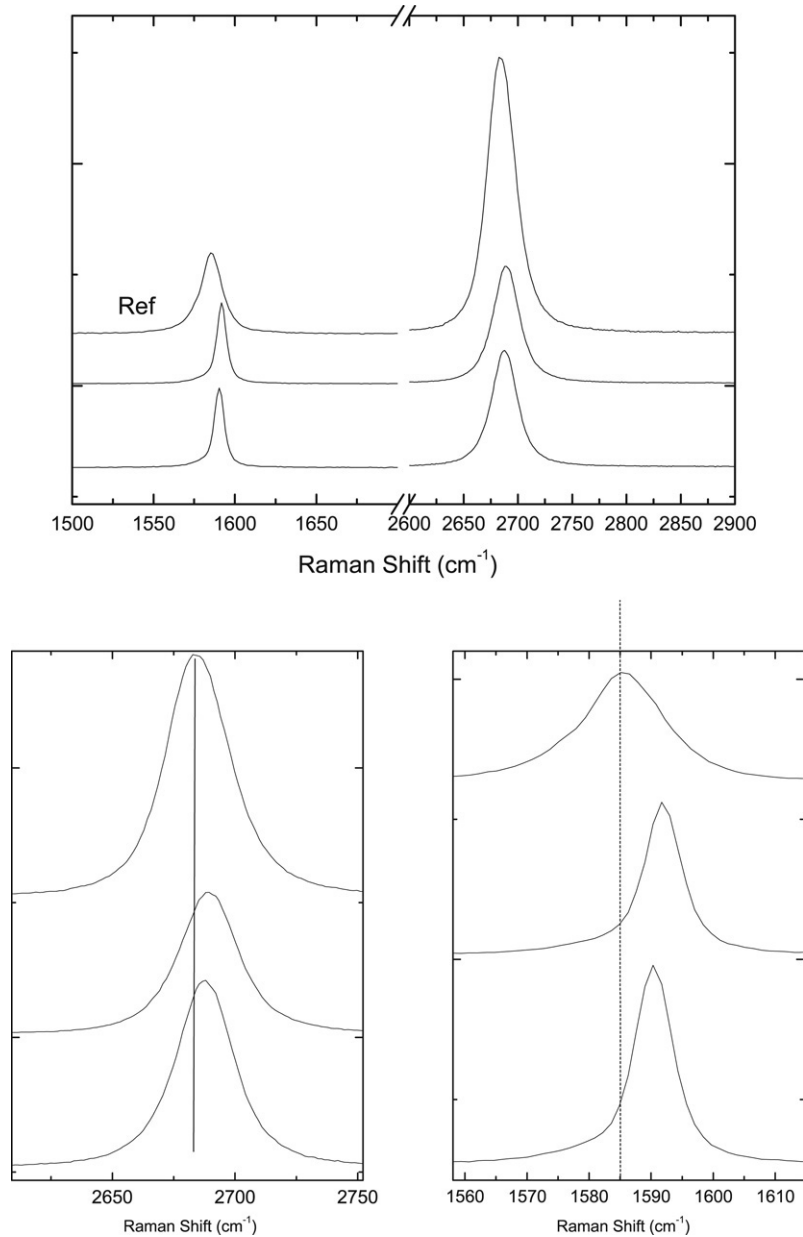


Fig. 9. Raman measurements in different points of a graphene sample.

fractions X_i and dimensions L_{ai} , the effective L_a is given by [13]:

$$\frac{1}{L_{a\text{Eff}}} = \sum_i^N X_i \frac{1}{L_{ai}}. \quad (9)$$

Thus, XRD weights more the bigger crystallites, while TK will underestimate L_a due to the dominant effect of small crystallites [93,95,98]. A recent study has fitted $C(\lambda) \sim 2.4 \times 10^{-10} \lambda^4$ [97], using $I(D)/I(G)$ as integrated areas ratio, rather than peak height ratios as in [26,91,44]. Using the area ratio gives different results since $\text{FWHM}(D)$ increases much more than $\text{FWHM}(G)$ for decreasing L_a [16,93].

The original idea behind Eq. (8) was to link the D peak intensity to phonon confinement. Thus, since the G peak is the allowed phonon, the intensity of the nonallowed phonon would

be ruled by the “amount of breaking” of the selection rule. This can be crudely estimated by the Heisenberg indetermination $\Delta q \Delta x \sim h$. Taking $\Delta x \sim L_a$, it is immediate to get Eq. (8). However, we now know that the activation of the D peak is due to double resonance and not just to phonon confinement. Considering L_a as an average interdefect distance, one can still assume that the higher the number of defects, the higher the D peak intensity and, thus, the smaller L_a . However, as things stand, a complete theory for the Raman intensity of the G and D peaks and their second orders is still lacking and is the subject of ongoing research [99]. Furthermore it would be ideal if a quantitative link to the number or nature of the defects could be established. This was not done in the past since the main interest in nanographites and carbon fibres was to have a rule of thumb estimation of disorder. However, in graphene the precise nature of the disorder and defects is of great interest, and their presence

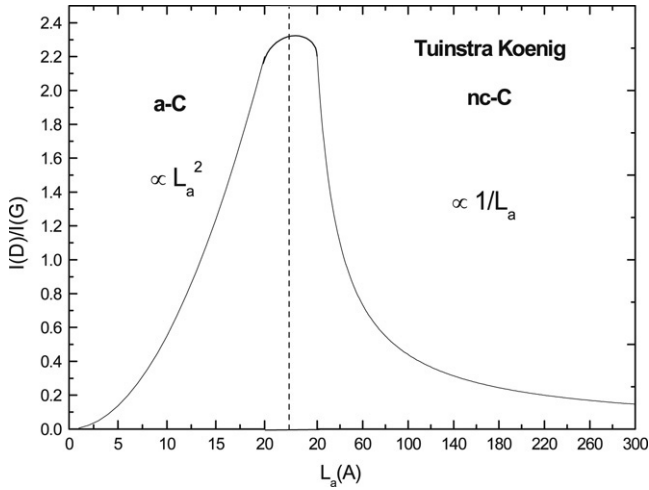


Fig. 10. Schematic evolution of $I(D)/I(G)$ as a function of disorder for visible excitation. The maximum of this curve is taken as boundary between nanocrystalline graphite and amorphous carbons [13].

can be linked to changes in the electrical characteristics. Thus a more detailed investigation is certainly needed.

The main effects in the evolution of the Raman spectrum in this stage are [13]:

- (a) The D peak appears and $I(D)/I(G)$ increases following (8);
- (b) D' peak appears at $\sim 1620 \text{ cm}^{-1}$;
- (c) All peaks FWHM broaden due to disorder;
- (d) The doublet structure of the D and $2D$ peak is lost.

For high disorder the broadening of the G and D' peaks is such that is often more convenient to consider a single G line, for practical purposes, when comparing different samples or the overall structural evolution of a given sample. The average G peak position then moves from ~ 1580 to $\sim 1600 \text{ cm}^{-1}$. The loss of three-dimensional ordering is indicated by the disappearance of the doublet in the D peak and in its second order [40].

Indeed, the doublet structure of the $2D$ peak has been shown to be a good indication of c axis ordering, and thus of turbostraticity. In particular, it was noted from early studies that turbostratic graphite, (i.e. without the planar AB stacking) has a single $2D$ peak [40]. However, its FWHM is $\sim 50 \text{ cm}^{-1}$ almost double that of the $2D$ peak of graphene and is upshifted of $\sim 20 \text{ cm}^{-1}$. Turbostratic graphite also often has a first order D peak [40].

(B) Stage 2: From nanocrystalline graphite to mainly sp^2 amorphous carbon

For an ever-increasing number of defects, including bond length and angle disorder at the atomic scale, the phonon modes will soften, particularly the G peak. The end of stage 2 corresponds to a completely disordered, almost fully sp^2 bonded a-C consisting of distorted sixfold rings or rings of other orders (with an upper limit of 20% sp^3). A typical example is sputtered amorphous carbon [100].

The main effects in the evolution of the Raman spectrum are:

- (a) G peak decreases from 1600 to $\sim 1510 \text{ cm}^{-1}$;

(b) TK is no longer valid: $I(D)/I(G) \propto M \propto L_a^2$;

(c) $I(D)/I(G) \rightarrow 0$;

(d) Increasing dispersion of the G peak.

Another effect is the absence of well-defined second-order Raman peaks, but a small modulated bump from ~ 2400 to $\sim 3100 \text{ cm}^{-1}$, Fig. 1.

The breakdown of TK is clear from Fig. 1. Amorphous carbons have a much smaller D peak intensity of what Eq. (8) would predict. The “molecular picture” helps in understanding what happens. For more disorder, clusters become smaller and the rings fewer and more distorted, until they begin to open up. As the G peak is just related to the relative motion of C sp^2 atoms, we can assume $I(G)$ roughly constant as a function of disorder. Thus, with the loss of sp^2 rings $I(D)$ will now decrease with respect to $I(G)$ and the TK relationship will no longer hold. For small L_a , the D mode strength is proportional to the probability of finding a sixfold ring in the cluster, i.e. to the cluster area. Thus, in amorphous carbons the development of a D peak indicates ordering, exactly the opposite to the case of graphite [13,14]. This is expressed in (b) above by the proportionality of $I(D)/I(G)$ to M , the number of ordered rings. This leads to a new relation for stage 2 [13], Fig. 10:

$$\frac{I(D)}{I(G)} = C'(\lambda) L_a^2. \quad (10)$$

Imposing continuity between (8) and (10), we find $C'(514 \text{ nm}) \approx 0.0055$.

In disordered carbons the G peak position increases as the excitation wavelength decreases, from IR to UV [14]. The dispersion rate increases with disorder. The G peak does not disperse in graphite itself, nanocrystalline (nc)-graphite or glassy carbon [13,14]. The G peak only disperses in more disordered carbons, where the dispersion is proportional to the degree of disorder. The G peak dispersion separates the materials into two types. In materials with only sp^2 rings, the G peak dispersion saturates at a maximum of $\sim 1600 \text{ cm}^{-1}$, the G position in nanocrystalline-graphite. In contrast, in those materials also containing sp^2 chains (typical of DLCs), the G peak continues to rise past 1600 cm^{-1} and can reach 1690 cm^{-1} at 229 nm excitation [14]. The D peak always disperses with excitation energy in all carbons [13,14]; however, the more disorder the less dispersion, opposite of the G peak [14].

7. Edges and ribbons

The sample edges can be always seen as defects. Thus, when the laser spot includes them, even if the bulk sample is perfect, a D peak will appear. Fig. 5 shows no D peak at the centre of a typical graphene layer, proving the absence of a significant number of defects in the structure. A single D peak is only observed at the sample edge, Fig. 11, consistent with the single $2D$ peak discussed in Section 4. On the other hand the D peak at the edge of graphite consists of two peaks D_1 and D_2 [36,38].

A detailed multiwavelength Raman investigation of graphene nanoribbons as a function of width should be done in the near future. However, it is immediate to think that a TK-like relation will link $I(D)/I(G)$ to the reciprocal of the ribbon width, at

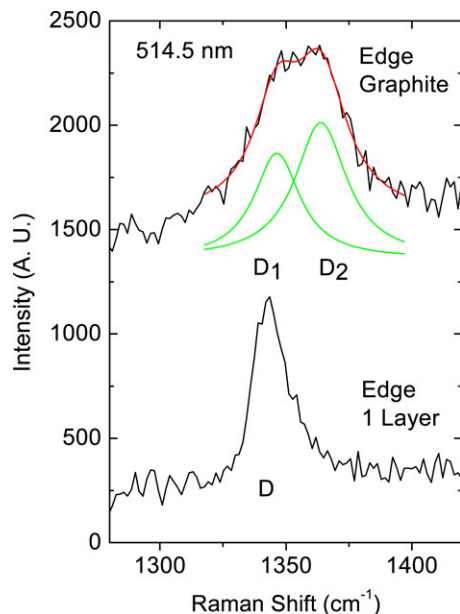


Fig. 11. Raman spectra of graphite and graphene edges.

least for ribbons significantly smaller than the laser spot. In this case, the smaller the ribbons, the more the edges, thus the bigger the D peak. However, the D peak could also increase due to disorder. Thus, two ribbons having similar widths, but different amounts of disorder will have different $I(D)/I(G)$.

For very small ribbons, phonon and electron confinement effects will become relevant and new modes will appear. A detailed theoretical and experimental investigation of the phonons in small ribbons is thus needed.

Finally the D peak intensity is maximum for polarization parallel to the edges, and is in principle selective to the edges chirality [28,101]. A detailed investigation will be reported later [90].

8. Conclusions

A review of the Raman spectra of graphite and graphene was presented. The G and $2D$ Raman peaks change in shape, position and relative intensity with number of graphene layers. This reflects the evolution of the electronic structure and electron–phonon interactions. Doping upshifts and sharpens the G peak for both holes and electrons. Disorder can be monitored via the D peak. Thus Raman spectroscopy can be efficiently used to monitor a number of layers, quality of layers, doping level and confinement in graphene nanostructures.

Acknowledgements

The author acknowledges S. Pisana, M. Lazzeri, C. Casiraghi, V. Scardaci, S. Piscanec, K.S. Novoselov, A.K. Geim, F. Mauri, J.C. Meyer, J. Robertson and funding from the Royal Society and The Leverhulme Trust.

References

[1] K.S. Novoselov, A.K. Geim, S.V. Morozov, D. Jiang, Y. Zhang, S.V. Dubonos, I.V. Grigorieva, A.A. Firsov, *Science* 306 (2004) 666.

[2] K.S. Novoselov, D. Jiang, F. Schedin, T. Booth, V.V. Khotkevich, S.V. Morozov, A.K. Geim, *Proc. Natl. Acad. Sci.* 102 (2005) 10451.
 [3] A.K. Geim, K.S. Novoselov, *Nat. Mater.* 6 (2007) 183.
 [4] J.C. Angus, C.C. Hayman, *Science* 241 (1988) 913.
 [5] H.W. Kroto, J.R. Heath, S.C. O'Brien, R.F. Curl, R.E. Smalley, *Nature* 318 (1985) 167.
 [6] S. Iijima, *Nature* 354 (1999) 56.
 [7] A. Oberlin, M. Endo, T. Koyama, *J. Cryst. Growth* 32 (1976) 335.
 [8] M. Monthieux, V.L. Kuznetsov, *Carbon* 44 (2006) 1621.
 [9] C. Casiraghi, J. Robertson, A.C. Ferrari, *Mater. Today* 10 (2007) 42.
 [10] R. Hauert, *Trib. Int.* 37 (2004) 991.
 [11] J.P. Sullivan, T.A. Friedmann, K. Hjort, *MRS Bull.* 26 (2001) 309.
 [12] A.C. Ferrari, *Surf. Coat. Technol.* 180–181 (2004) 190.
 [13] A.C. Ferrari, J. Robertson, *Phys. Rev. B* 61 (2000) 14095.
 [14] A.C. Ferrari, J. Robertson, *Phys. Rev. B* 64 (2001) 075414.
 [15] C. Casiraghi, A.C. Ferrari, J. Robertson, *Phys. Rev. B* 72 (2005) 085401.
 [16] A.C. Ferrari, S.E. Rodil, J. Robertson, *Phys. Rev. B* 67 (2003) 155306.
 [17] B. Racine, A.C. Ferrari, N.A. Morrison, I. Hutchings, W.I. Milne, J. Robertson, *J. Appl. Phys.* 90 (2001) 5002.
 [18] M. Endo, T. Hayashi, Y.A. Kim, H. Muramatsu, *Jpn. J. Appl. Phys.* 45 (2006) 4883.
 [19] A.C. Ferrari, J. Robertson (Eds.), *Raman spectroscopy in carbons: From nanotubes to diamond*. *Philos. Trans. R. Soc. Ser. A* 362, 2267–2565.
 [20] C. Berger, Z. Song, T. Li, X. Li, A.Y. Ogbazghi, R. Feng, Z. Dai, A.N. Marchenkov, E.H. Conrad, P.N. First, W.A. de Heer, *J. Phys. Chem. B* 108 (2004) 19912.
 [21] C. Oshima, A. Nagashima, *J. Phys. C* 9 (1997) 1.
 [22] R. Rosei, S. Modesti, F. Sette, *Phys. Rev. B* 29 (1984) 3416.
 [23] S. Stankovich, D.A. Dikin, G.H.B. Dommett, K.M. Kohlhaas, E.J. Zimney, E.A. Stach, R.D. Piner, S.T. Nguyen, R.S. Ruoff, *Nature* 442 (2006) 282.
 [24] M.J. O'Connell, S.M. Bachilo, C.B. Huffman, V.C. Moore, M.S. Strano, E.H. Haroz, K.L. Rialon, P.J. Boul, W.H. Noon, C. Kittrell, J. Ma, R.H. Hauge, R.B. Weisman, R.E. Smalley, *Science* 297 (2002) 593.
 [25] P. Patsalas, M. Handrea, S. Logothetidis, M. Gioti, S. Kennou, W. Kautek, *Diam. Relat. Mater.* 10 (2001) 960.
 [26] F. Tuinstra, J.L. Koenig, *J. Chem. Phys.* 53 (1970) 1126.
 [27] Y. Gogotsi, J.A. Libera, N. Kalashnikov, M. Yoshimura, *Science* 290 (2000) 317.
 [28] L.G. Cancado, M.A. Pimenta, B.R.A. Neves, G. Medeiros-Ribeiro, E. Toshiaki, Y. Kobayashi, K. Takai, K. Fukui, M.S. Dresselhaus, R. Saito, A. Jorio, *Phys. Rev. Lett.* 93 (2004) 047403.
 [29] A.C. Ferrari, J.C. Meyer, V. Scardaci, C. Casiraghi, M. Lazzeri, F. Mauri, S. Piscanec, D. Jiang, K.S. Novoselov, S. Roth, A.K. Geim, *Phys. Rev. Lett.* 97 (2006) 187401.
 [30] S. Pisana, M. Lazzeri, C. Casiraghi, K.S. Novoselov, A.K. Geim, A.C. Ferrari, F. Mauri, *Nat. Mater.* 6 (2007) 198.
 [31] A.C. Ferrari, J. Robertson, *Phys. Rev. B* 63 (2001) 121405.
 [32] N. Wada, P.J. Gaczi, A. Solin, *J. Non-Cryst. Solids* 35–36 (1980) 543.
 [33] S.R. Salis, D.J. Gardiner, M. Bowden, J. Savage, D. Rodway, *Diam. Relat. Mater.* 5 (1996) 589.
 [34] C. Castiglioni, F. Negri, M. Rigolio, G. Zerbi, *J. Chem. Phys.* 115 (2001) 3769.
 [35] C. Castiglioni, M. Tommasini, G. Zerbi, *Philos. Trans. R. Soc. Lond. Ser. A* 362 (2004) 2425.
 [36] R.J. Nemanich, S.A. Solin, *Phys. Rev. B* 20 (1979) 392.
 [37] R. Al-Jishi, G. Dresselhaus, *Phys. Rev. B* 26 (1982) 4514.
 [38] R.P. Vidano, D.B. Fishbach, L.J. Willis, T.M. Loehr, *Solid State Commun.* 39 (1981) 341.
 [39] I. Pocsik, M. Hundhausen, M. Koos, L. Ley, *J. Non-Cryst. Solids* 227–230 (1998) 1083.
 [40] P. Lespade, A. Marchard, M. Couzi, F. Cruege, *Carbon* 22 (1984) 375.
 [41] C. Thomsen, S. Reich, *Phys. Rev. Lett.* 85 (2000) 5214.
 [42] A.V. Baranov, A.N. Bekhterev, Y.S. Bobovich, V.I. Petrov, *Opt. Spektrosk.* 62 (1987) 1036.
 [43] C. Mapelli, C. Castiglioni, G. Zerbi, K. Mullen, *Phys. Rev. B* 60 (1999) 12710.

- [44] M.J. Matthews, M.A. Pimenta, G. Dresselhaus, M.S. Dresselhaus, M. Endo, *Phys. Rev. B* 59 (1999) 6585.
- [45] A. Grüneis, R. Saito, T. Kimura, L.G. Cançado, M.A. Pimenta, A. Jorio, A.G. Souza Filho, G. Dresselhaus, M.S. Dresselhaus, *Phys. Rev. B* 65 (2002) 155405.
- [46] R. Saito, A. Jorio, A.G. Souza Filho, G. Dresselhaus, M.S. Dresselhaus, M.A. Pimenta, *Phys. Rev. Lett.* 88 (2002) 027401.
- [47] J. Maultzsch, S. Reich, C. Thomsen, H. Requardt, P. Ordejón, *Phys. Rev. Lett.* 92 (2004) 075501.
- [48] S. Piscanec, M. Lazzeri, F. Mauri, A.C. Ferrari, J. Robertson, *Phys. Rev. Lett.* 93 (2004) 185503.
- [49] G. Kresse, J. Furthmüller, J. Hafner, *Europhys. Lett.* 32 (1995) 729.
- [50] P. Pavone, R. Bauer, K. Karch, O. Schütt, S. Vent, W. Windl, D. Strauch, S. Baroni, S. de Gironcoli, *Physica B* 219–220 (1996) 439.
- [51] O. Dubay, G. Kresse, *Phys. Rev. B* 67 (2003) 035401.
- [52] L. Wirtz, A. Rubio, *Solid. State Commun.* 131 (2004) 141.
- [53] M. Lazzeri, S. Piscanec, F. Mauri, A.C. Ferrari, J. Robertson, *Phys. Rev. B* 73 (2006) 155426.
- [54] W. Kohn, *Phys. Rev. Lett.* 2 (1959) 393.
- [55] S. Piscanec, M. Lazzeri, J. Robertson, A.C. Ferrari, F. Mauri, *Phys. Rev. B* 75 (2007) 035427.
- [56] Z. Yao, C.L. Kane, C. Dekker, *Phys. Rev. Lett.* 84 (2000) 2941.
- [57] J.Y. Park, S. Rosenblatt, Y. Yaish, V. Sazonova, H. Ustunel, S. Braig, T.A. Arias, P.W. Brouwer, P.L. McEuen, *Nano Lett.* 4 (2004) 517.
- [58] M. Lazzeri, S. Piscanec, F. Mauri, A.C. Ferrari, J. Robertson, *Phys. Rev. Lett.* 95 (2005) 236802.
- [59] V. Perebeinos, J. Tersoff, P. Avouris, *Phys. Rev. Lett.* 94 (2005) 086802.
- [60] A. Javey, J. Guo, M. Paulsson, Q. Wang, D. Mann, M. Lundstrom, H. Dai, *Phys. Rev. Lett.* 92 (2004) 106804.
- [61] J. Jiang, R. Saito, A. Grüneis, G. Dresselhaus, M.S. Dresselhaus, *Chem. Phys. Lett.* 392 (2004) 383.
- [62] G.D. Mahan, *Phys. Rev. B* 68 (2003) 125409.
- [63] G. Pennington, N. Goldsman, *Phys. Rev. B* 68 (2004) 045426.
- [64] J. Jiang, R. Saito, A. Grüneis, S.G. Chou, Ge.G. Samsonidze, A. Jorio, G. Dresselhaus, M.S. Dresselhaus, *Phys. Rev. B* 71 (2005) 045417.
- [65] S. Koswatta, S. Hasan, M.S. Lundstrom, M.P. Anantram, D.E. Nikonov, *cond-mat/0511723*, 2005.
- [66] S.Y. Zhou, G.H. Gweon, J. Graf, A.V. Fedorov, C.D. Spataru, R.D. Diehl, Y. Kopelevich, D.-H. Lee, S.G. Louie, A. Lanzara, *Nat. Phys.* 2 595 (2006).
- [67] K.S. Novoselov, A.K. Geim, S.M. Morozov, M.I. Katsnelson, I.V. Grigorieva, S.V. Dubonos, A.A. Firsov, *Nature* 438 (2005) 197.
- [68] R. Nicklow, N. Wakabayashi, H.G. Smith, *Phys. Rev. B* 5 (1972) 4951.
- [69] C. Oshima, T. Aizawa, R. Souda, Y. Ishizawa, Y. Sumiyoshi, *Solid State Commun.* 65 (1988) 1601.
- [70] S. Siebentritt, R. Pies, K.-H. Rieder, A.M. Shikin, *Phys. Rev. B* 55 (1997) 7927.
- [71] P.H. Tan, C.Y. Hu, J. Dong, W.C. Shen, B.F. Zhang, *Phys. Rev. B* 64 (2000) 214301.
- [72] V. Scardaci, A.C. Ferrari, et al., (unpublished).
- [73] M. Lazzeri, F. Mauri, *Phys. Rev. Lett.* 97 (2006) 266407.
- [74] A. Gupta, G. Chen, P. Joshi, S. Tadigadapa, P.C. Eklund, *Nano Lett.* 6 (2006) 2667.
- [75] D. Graf, F. Molitor, K. Ensslin, C. Stampfer, A. Jungen, C. Hierold, L. Wirtz, *Nano Lett.* 7 (2007) 238.
- [76] L.G. Cancado, M.A. Pimenta, R. Saito, A. Jorio, L.O. Ladeira, A. Grueneis, A.G. Souza-Filho, G. Dresselhaus, M.S. Dresselhaus, *Phys. Rev. B* 66 (2002) 035415.
- [77] A. Jorio, C. Fantini, M.S. Dantas, M.A. Pimenta, A.G. Souza Filho, G. Samsonidze, V.W. Brar, G. Dresselhaus, M.S. Dresselhaus, A.K. Swan, M.S. Unlu, B. Goldberg, R. Saito, *Phys. Rev. B* 66 (2002) 115411.
- [78] J. Maultzsch, S. Reich, C. Thomsen, *Phys. Rev. B* 70 (2004) 155403.
- [79] J. Yan, Y. Zhang, P. Kim, A. Pinczuk, *Cond.Mat./0612634*, 2006.
- [80] T. Ando, *J. Phys. Soc. Japan* 75 (2006) 124701.
- [81] A.H. Castro Neto, F. Guinea, *Phys. Rev. B* 75 (2007) 045404.
- [82] M. Born, J.R. Oppenheimer, *Ann. Phys.* 84 (1927) 457.
- [83] J.M. Ziman, *Electrons and Phonons*, Oxford Univ. Press, Oxford, 1960.
- [84] G. Grimvall, *The Electron-Phonon Interaction in Metals*, North-Holland, Amsterdam, 1981.
- [85] Y. Zhang, Z. Jiang, J.P. Small, M.S. Purewal, Y.W. Tan, M. Fazlollahi, J.D. Chudow, J.A. Jaszczak, H.L. Stormer, P. Kim, *Phys. Rev. Lett.* 96 (2006) 136806.
- [86] G. Moos, C. Gahl, R. Fasel, M. Wolf, T. Hertel, *Phys. Rev. Lett.* 87 (2001) 267402.
- [87] T. Kampfrath, L. Perfetti, F. Schapper, C. Frischkorn, M. Wolf, *Phys. Rev. Lett.* 95 (2005) 187403.
- [88] L. Pietronero, S. Strassler, *Phys. Rev. Lett.* 47 (1981) 593.
- [89] A. Das, S. Pisana, A.K. Sood, A.C. Ferrari, et al., 2007 (unpublished).
- [90] C. Casiraghi, A.C. Ferrari, et al., 2007 (unpublished).
- [91] D.S. Knight, W.B. White, *J. Mater. Res.* 4 (1989) 385.
- [92] K. Sinha, J. Menendez, *Phys. Rev. B* 41 (1990) 10845.
- [93] A. Cuesta, P. Dhamelincourt, J. Laureyns, A. Martinez-Alonso, J.M.D. Tascon, *J. Mater. Chem.* 8 (1998) 2875.
- [94] P. Lespade, R. Al-Jishi, M.S. Dresselhaus, *Carbon* 20 (1982) 427.
- [95] H. Wilhelm, M. Lelaurain, E. McRae, B. Humbert, *J. Appl. Phys.* 84 (1998) 6552.
- [96] Y. Wang, D.C. Alsmeyer, R.L. McCreery, *Chem. Mater.* 2 (1990) 557.
- [97] L.G. Cançado, K. Takai, T. Enoki, M. Endo, Y.A. Kim, H. Mizusaki, A. Jorio, L.N. Coelho, R. Magalhães-Paniago, M.A. Pimenta, *Appl. Phys. Lett.* 88 (2006) 163106.
- [98] N. Nakamizo, R. Kammereck, P.L. Walker Jr., *Carbon* 12 (1974) 259.
- [99] K. Sato, R. Saito, Y. Oyama, J. Jiang, L.G. Cançado, M.A. Pimenta, A. Jorio, Ge.G. Samsonidze, G. Dresselhaus, M.S. Dresselhaus, *Chem. Phys. Lett.* 427 (2006) 117.
- [100] F. Li, J.S. Lannin, *Phys. Rev. Lett.* 65 (1990) 1905.
- [101] L.G. Cancado, M.A. Pimenta, B.R.A. Neves, M.S.S. Dantas, A. Jorio, *Phys. Rev. Lett.* 93 (2004) 247401.